CHARACTERIZATION AND EVALUATION OF CARBON NANOTUBE BUCKY-PAPER MEMBRANES FOR DIRECT CONTACT MEMBRANE DISTILLATION

Ludovic F. Dumée[1,2,#], Kallista Sears[1#], Jürg Schütz[1], Niall Finn[1], Chi Huynh[1], Stephen Hawkins[1]
Mikel Duke[2], Stephen Gray[2]
[1] CSIRO Materials Science and Engineering, Bayview Ave, Clayton Vic 3168, Australia
[2] Victoria University Werribee Campus, Hoppers Lane, Werribee PO Box 14428 Melbourne, Victoria, 8001, Australia
Tel: +61 (0)3 9545 2107 - Fax: +61 (0)3 9545 2363 # corresponding authors: ludovic.dumee@csiro.au & kallista.sears@csiro.au

ABSTRACT

Self-supporting carbon nanotube (CNT) Bucky-Papers have unique structural and surface properties which can be utilised in many applications. In this work we characterised pure self-supporting CNT membranes, where CNTs were held together only by Van der Waals forces, and evaluated their potential and performance in direct contact membrane distillation. The membranes were found to be highly hydrophobic (contact angle of 113°), highly porous (90%), and to exhibit a thermal conductivity of 2.7 kW/m^2•h. We demonstrate, as a proof of concept, that self-supporting CNT Bucky-Paper membranes can be used for desalination in a direct contact membrane distillation setup with 99% salt rejection and a flux rate of ~12 kg/m^2*h at a water vapour partial pressure difference of 22.7kPa. Ageing of the membranes by delamination, factor limiting their performance, is also reported but work is currently done to address this issue by investigating composite material structures.

Keywords: carbon nanotube, bucky-paper, membrane, direct contact membrane distillation, desalination

1. INTRODUCTION

Growing concern over our finite and stressed water resources has led to renewed interest into Membrane Distillation (MD) as an alternative method for water purification and desalination. MD is a thermally driven process based on a vapour pressure gradient across a hydrophobic membrane [1,] [2]. The most commonly used configuration is Direct Contact Membrane Distillation (DCMD) in which a hydrophobic membrane acts as a barrier between a feed of hot seawater or brackish water and a permeate of cold freshwater (Figure 1 ~~Figure 1~~). While liquid cannot cross the membrane, water vapour is able to travel through the pores driven by the difference in water vapour partial pressure. Previous studies have shown that even small temperature differences between the feed and permeate can lead to significant fluxes [3].

In contrast to other desalination techniques such as nanofiltration and reverse osmosis, DCMD offers a potentially low energy and high rejection route to the desalination of highly dirty or salty waters. However, to become competitive with other desalination technologies, the DCMD process needs to be improved ~~and~~ with membranes tailored specifically for this application. Two main membrane properties are critical for DCMD. Firstly, in order to achieve efficient vapour transport from the hot to the cold side, the membrane needs to be highly porous and as thin as possible [4-5]. Secondly, the pores need to be large enough to facilitate vapour transport, while having sufficiently small dimensions to avoid membrane wetting and formation of a direct liquid bridge between the feed and the permeate sides [2-6]. Most previous studies have investigated membranes formed from Poly(propylene) (PP), Poly(vinylidene-fluoride) (PVDF) and Poly(tetrafluoroethylene) (PTFE) [7]. While these materials are highly hydrophobic, they are also expensive and difficult to process. It is consequently important to investigate other alternatives as well as techniques for improving the process efficiency by modifying the membrane properties and structure.

One possibility is to explore Carbon Nanotube (CNT) based membranes. CNTs are nano-scale cylinders of rolled up graphene with inner diameters as small as 0.7 nm (Figure 2 ~~Figure 2~~). They have exceptional mechanical, electrical and thermal properties, and it was recently revealed that they exhibit fast fluid flow through their interior. This has stimulated intense interest in CNT based membranes of various structures [8-11]. In this work we focus on CNT Bucky-Paper (BP) membranes, which is a paper-like structure of CNTs processed by vacuum filtration [12]. We then apply CNT BP membranes to the novel application of MD.

For the application of MD, the properties surrounding the nanotubes are of key interest. Here we utilise various microscopy, porosimetry, surface and physical property analytical devices

to uncover valuable features of the CNT BP membranes and relate this to performance in MD. The CNT BP membranes have been characterised using various techniques including scanning electron microscopy (SEM), transmission electron microscopy (TEM), ~~Nitrogen~~ nitrogen adsorption, contact angle measurements, mechanical tensile tests, and thermal conductivity measurements. They were also tested against commercial PTFE membranes.

2. THEORY

Theoretical derivations around MD mass and energy transport are well described [13]. Here we present the relevant theory for our study. Two properties, permeance, *f,* and permeability, *k*, are used to quantify mass transport across a membrane and are defined as:

$$f = \frac{J}{A \times \Delta P} \quad (1)$$

$$k = \frac{J \times L}{A \times \Delta P} \quad \textbf{(2)}$$

where *J* (kg/s) is the flux through the membrane, *L* (m) the membrane thickness, *A* (m^2) the membrane area and, in the case of membrane distillation, ΔP (Pa) is the difference in water vapour partial pressure across the membrane. The permeance can be determined by taking the gradient of a plot of flux against the vapour pressure difference, and dividing by the membrane area. The permeability is simply the permeance multiplied by the membrane thickness.

If the temperatures of the hot and cold streams are known, the water vapour partial pressure can be estimated based on Antoine's equation:

$$P = e^{\left(23.328 - \frac{3841}{T-45}\right)} \quad \textbf{(3)}$$

where the vapour partial pressure *P* is in Pa and the temperature T in Kelvin (K).

For direct contact membrane distillation it is generally accepted that mass transport through the membrane can operate in one of three regimes: (i) Knüdsen flow, (ii) molecular flow or (iii) a combination of both known as transition flow. The dominating regime is indicated by the Knüdsen number (K_n), defined as the ratio of the mean free path (λ) to the pore diameter (d) [14-16]. The mean free path is defined as:

$$\lambda = \frac{RT}{\sqrt{2}\pi d^2 N_A P} \quad \textbf{(4)}$$

where R is the Boltzmann constant, T the temperature in Kelvin, d the average particle diameter, N_A the Avogadro number and P the working pressure.

For Knüdsen numbers, $K_n > 1$, the molecule - pore wall collisions dominate leading to Knüdsen type flow: For isoporous membranes with circular pores the permeance is given by [7-17]:

$$f_K = \frac{2}{3} \times \sqrt{\frac{8M}{\pi R T_a}} \times \left(\frac{r\varepsilon}{\tau\delta} \right) \quad \textbf{(5)}$$

where R represents the gas constant (J×K^{-1}×mol^{-1}), M the molar mass (g×mole^{-1}), T_a the average temperature (K), r the average pore radius, δ the membrane thickness (m), τ, the tortuosity and ε, the membrane porosity.

At the other extreme, for K_n<0.01, molecule-molecule collisions dominate leading to molecular flow through the stagnant air film trapped in the membrane. The permeance is then given by:

$$f_M = \frac{P_T D M}{R T_a} \frac{1}{P_{\ln}} \frac{\varepsilon}{\tau\delta} \quad \textbf{(6)}$$

where D is the diffusivity of water vapour in air, P_T is the total pressure (air and water vapour) within the membrane and is assumed to be 101.325 kPa in this work, P_{ln} is the mean log average of the air pressure in the membrane defined as:

$$P_{\ln} = \frac{P_{air2} - P_{air1}}{\ln\left(\frac{P_{air1}}{P_{air2}} \right)} \quad \textbf{(7)}$$

where P_{air1} and P_{air2} represent the air partial pressure at the hot and cold side of the membrane respectively.

At intermediate Knüdsen numbers 1>K_n>0.01, a combination of both transport mechanisms can occur. The total resistivity of the system is then equal to the sum of both Knüdsen and Molecular resistivity. This was modelled as resistances in series in previous studies [15], leading to the following equation for permeance:

$$f_T = \frac{1}{1/f_K + 1/f_M} \quad \textbf{(8)}$$

Furthermore, the temperature polarisation coefficient as a function of feed temperature is given by the equation:

$$\theta = \frac{T_1^m - T_2^m}{T_1^b - T_2^b} \quad \textbf{(9)}$$

where the subscripts 1 and 2 refer to the hot and the cold side, respectively, T^m stands for the temperature of the membrane surface and T^b is the temperature in the bulk solution, which is taken as the average of the inlet and outlet temperatures.[.1]

3. EXPERIMENTAL DETAILS

3.1 Material and processing

The CNTs were grown by chemical vapor deposition. A 1-5 nm thick iron catalyst film was deposited onto a silicon substrate bearing a thin Silicon Dioxide layer. A mixture of Helium (95%) - Acetylene (5%) was used as the carbon feedstock and heated to between 650 and 750°C. The CNTs typically have an outer diameter of ~10-15 nm (Figure 2~~Figure 2~~) and length of 150-300 µm [18].

The CNT BP membranes were processed by vacuum filtration of CNTs dispersed in 99.8% pure propan-2-ol [19]. Well dispersed CNT suspensions were obtained by repeated sonication for 15 minute intervals at a power of 150 W. Vacuum filtration was performed with a 47 mm diameter Millipore filtration unit with house line vacuum (dP= -95 kPa). The CNTs were filtered onto a Poly(ethersulphone) (PES) 0.2 µm-pore size Millipore membrane and then pealed off to form a self-supporting membrane.

PTFE membranes with 0.22 µm pore size were purchased from Millipore and tested for comparison. The PTFE membranes were composed of a thin (~ 30 µm) layer of pure stretched PTFE on a poly-ethylene grid support.

3.2 Membrane characterisation techniques

3.2.1 Pore size

Three complementary techniques were used to characterise pore size. Firstly a surface apparent pore size was determined from SEM images taken with a Philips FEG SEM at 2 kV. Each image was taken under the same conditions to reduce errors when comparing pore sizes between membranes. At least 3 images per sample were taken and the scans were performed at low frequencies (120 mS) to increase the pixel content. The CNTs were sufficiently conductive to not require metal coating which also avoided any additional error in the pore size estimation. The images were analysed using the software, ISIS and the edge-pores were not taken in consideration for the calculations. The minimum, mean and maximum average pore size distributions were calculated using Feret's approach [13-20]. In this method, 3 diameters are calculated for each pore, corresponding namely to the minimum, the mean and the maximum pore size, which gives information on pore shape distribution. However, this method only presents a surface apparent pore size and other tests were required to confirm the pore size distribution.

The second method relied on particle size exclusion tests to determine the particle size cut off. These tests were performed by filtrating Bovine Serum Albumin (BSA) and nano-particles

(purchased from Sigma Aldrich) through the Bucky-paper membranes. BSA has an average diameter of 5 nm while the nano particle diameters were 50nm (polystyrene-amine modified), 100 nm (polystyrene-sulphate modified) and 500 nm (polystyrene-sulphate modified). The particle diameter distribution was measured using a Zeta Sizer and agreed well with the manufacturer's specifications. The solute concentration was analysed either by UV-vis spectrophotometry or Fluorescence spectrophotometry depending on the ~~reactivity~~ absorption characteristics of the components.

Finally, porometer measurements were made on a Capillary Flow Porometer from Porous Material Inc, NY USA. In addition to pore size distribution this also provides a bubble point measurement for the membranes.

3.2.2 Membrane porosity

The membrane porosity was measured using a 2 mL pycnometer following the procedure outlined by Smolders et al. [5]. A minimum of 3 samples was used to calculate the average porosity. The experiment involved measuring the mass of sample in two different liquids. The first liquid (propan-2-ol) wets the membrane and enters the pores, while the second liquid (deionised water) does not wet or fill the pores. Once immersed, the sample was left for 20 mins and then sonicated for 2 mins at low power (150 W and 20ºC) to remove any trapped air bubbles. Furthermore, prior to changing liquids the sample was dried in a vacuum oven for 20 mins. The porosity was then calculated according to:

$$\varepsilon = 1 - \frac{\rho_b}{\rho_a} * \frac{(M_1 + M_2^a - M_3^a)}{(M_1 + M_2^b - M_3^b)} \quad \textbf{(10)}$$

where ε is the porosity, the superscripts a and b correspond respectively to isopropanol and water, respectively, ρ is the liquid density, M_1 is the mass of the dry sample, M_2 is the mass of the bottle filled with liquid ,and M_3 is the mass of the bottle plus sample filled with liquid.

3.2.3 Surface area

An average BET surface area was determined by N_2 adsorption on a Micromeretics Tristar 3000 [21]. The samples were first degassed for 70 hours and then analysed at 77 K.

3.2.4 Thickness and cross section

An FEI Nova nanolab 200 Dual Beam Focused Ion Beam (FIB) was used to form cross sections of the BP membranes. Milling was performed with a 1 nA, 30 kV Ga ion beam, followed by 0.3 nA cleaning steps.

3.2.5 Thermal conductivity

Thermal conductivity tests were preformed on 100 μm thick BP using an Armfield Limited

Thermal conductivity meter HT1-A. The samples were placed between two copper cylinders. A correlation between the power provided to the circuit and the thermal conductivity can be calculated according to:

$$\lambda_{th} = \frac{\Pi \times \delta}{A_{contact}} \quad \textbf{(11)}$$

Where λ is the thermal conductivity ($W \times m^{-1} \times K^{-1}$), Π the input power (W), δ the thickness (m) and A the area of contact (m^2) of the sample with the copper cylinders. The power used was 10 W and the cooling water temperature was 12ºC. Stable measurements were achieved within 5 mins for each sample.

3.2.6 Tempearature polarisation

The temperature at the membrane surface was estimated by placing a thermocouple in contact with the membrane surface at the centre of the module and on both sides of the membrane. The thermocouples were sandwiching the membrane without damaging it and the tests were done at 6 different hot side temperatures ranging from 25ºC to 85ºC. [.2]

Furthermore, another experiment where the feed/permeate ~~flux~~ flowrates were changed while keeping the other parameters cstant, such as temperatures and conductivities ~~constant,~~ was performed. The feed and permeate ~~flux~~ flowrate were kept ~~similar~~ equal for all the DCMD tests. In this configuration, the changes in flux across the membrane were recorded as a function of the feed ~~flux~~flowrate. Tests were performed at hot and cold temperatures of respectively 80ºC and 5ºC ~~and~~ with synthetic seawater.

3.2.7 Mechanical tensile behaviour

Tensile mechanical tests of the self-standing BPs were performed on an Instron with a 10 N load cell and a 2.5 mm/min rate of extension. The sample strips were 10 mm in length and 2 - 2.5 mm in width.

3.2.8 Contact angle

A pocket goniometer PG-3 from Fibro Systems was used to determine contact angle. The tests were performed in dynamic mode at 20ºC with 4 µL drops of deionised water [22] and over 10 min. Each type of membrane was tested at least 3 times.

3.2.9 Limit entry pressure (LEP) and bubble point

LEP tests were performed in an Amicon cell. The pressure was increased in 5 psi increments and the samples maintained at each pressure for 10 mins. Bubble point measurements were done with methanol following ASTM F316. The Bubble Point was also characterised with a Porometer (cf. 3.2.1).

3.3 Direct contact membrane distillation setup

A schematic of the test rig is shown in Figure 3. A peristaltic pump (Cole Palmer Masterflex, model 7521-25) fitted with two coupled heads (Easyload II, Model 77200-60) was used. The heater (CS Lauda C6) and cooler (Thermo Scientific Neslab RTE-7) enabled a wide range of operating temperatures. The electrical conductivity and temperature of the hot and cold electrolytes as well as the water level transferred to the cold side were monitored over time. Tests were performed in a PTFE module in counter current flow, with deionised water, on the cold side, and synthetic seawater on the hot one (35 g/L NaCl solutions). The cell was cylindrical, with a diameter and height of 25 mm and 2 mm respectively. The flow rate for each ~~head~~ stream was kept at 200 mL/min unless otherwise stated, [.3]while the temperatures of the ~~water~~ feed streams were kept constant. The membrane test~~ed~~ area was a disc of 25.4 mm ~~of~~ diameter[.4]. No major temperature drop~~s~~ between the inlet and the outlet of the module were recorded and the temperature was considered constant over the membrane.[.5]

The permeate was measured by observing the increase in volume of th cold permeate flow via a graduated micro-burette. The micro-burette was placed in the permeate line etc. [.6]

4. RESULTS

4.1 Membrane characterisation

The structure of the BP membrane was clearly discerned from SEM images of the surface, such as in Figure 4~~Figure 4~~ (a) and (b), and of cross-sections milled by Focused Ion Beam (FIB), as presented in Figure 4~~Figure 4~~.(c). The BP membrane was essentially a mat of randomly entangled CNTs. Furthermore the cross-sectional images showed that the CNTs tend to form a layered structure with very few CNTs aligned perpendicular to the surface. The surface was relatively smooth with a roughness ranging from a few hundred nanometres to a few micrometers, as visible in Figure 4~~Figure 4~~ (a). Thanks to the well dispersed CNT suspensions, the membrane surface and cross section were uniform and free from large CNT-bundles [8].

Three techniques were used to characterise the pore size of the BP membranes. SEM images yielded to a surface apparent pore size distribution as shown in Figure 5~~Figure 5~~. This gave an average pore size of ~22 nm with ~95% of the pores falling below 70 nm. This value compared well with the particle size exclusion test, where a cut off of >50 nm was determined by filtration of latex beads as presented in Figure 6~~Figure 6~~.

One of the most important membrane parameters is its thermal conductivity which directly

impacts the process efficiency. Most of the heat transferred across the membrane should be carried with the vapour and heat losses due to conduction through the membrane material should be minimised. Using the thermal conductivity meter, the thermal conductivity of the BPs was measured to be ~2.7 $W \times m^{-2} \times K^{-1}$. This is low in comparison to the high thermal conductivities (~700 $W \times m^{-2} \times K^{-1}$) that have been predicted and reported for individual multi-walled CNTs [23-25]. For MD, this smaller conductivity is preferred from a performance point of view. The difference is likely due to the high porosity of the membrane structure combined with the BP's layer structure and the relatively poor heat conductivity at interconnects between CNTs. Other experiments are under way to fully characterize the thermal behaviour of the BP structures. As a comparison, tested PTFE membranes show conductivities ~0.25 $W \times m^{-2} \times K^{-1}$, 10 times lower than the BP but half of that of other polymeric membranes of similar pore size such as PES or poly(~~vynil~~vinylidenei fluoride~~ure~~) [.7](PVDF).

Various other techniques were also used to characterise the membranes and determine their suitability for membrane distillation. These results are summarised in Table 1~~Table 1~~ and where possible are also compared with values for a typical PTFE membrane. Table 1~~Table 1~~ shows that the BP membrane properties are generally comparable to those of the PTFE membrane making them a promising candidate for MD. For example, pycnometer tests indicated a porosity of 90%, exceeding the 70% measured for PTFE. The BP membrane also exhibited a high contact angle of ~113 ° close to that of PTFE (120 °).

4.2 DCMD

4.2.1 Flux and permeability

A number of PTFE and BP membranes were tested in a DCMD setup. The test conditions and membrane details are given in Table 2~~Table 2~~.

Figure 7~~Figure 7~~ illustrates how the flux varies over time for representative PTFE and BP membranes. PTFE membranes are amongst the best available for MD [26] and as expected, the flux reaches steady state after an initial settling period of ~15-20 min. The BPs on the other hand behaved differently. The flux initially increased over the first 15 min before stabilising. However, this stabilisation is often followed by a slow decline until the membrane breaks. The origin of this declining flux is still uncertain. It may be related to temperature polarisation as the BP membranes have a thermal conductivity 10 times higher than that of PTFE but lower than PVDF. However, preliminary experiments seem to indicate that temperature polarisation (equation 9) is not a severe effect.

For all feed temperatures investigated, similar temperature polarisation coefficients were measured for both PTFE and BP membranes and were always greater than 0.9 (Figure 9). This

seems to indicate that temperature polarisation ~~is~~ was not a dominant effect.

To confirm this result a 110μm thick BP was tested under constant temperatures but with changing feed and permeate flow rates (Figure 10). Both feed and permeate flow rates were equal and varied between tests from 0.15 to 0.4 kg/min but ~~was kept constant for both feed and permeate~~. The flux across the membrane is clearly increasing with increasing feed/permeate ~~flux~~flowrate, corresponding to ~~a more~~greater turbulence and lower ~~t flux~~temperature polarisation. For a ~~doubled~~ doubling of the flow rate, the flux across the membrane ~~is~~ was also ~~practically~~ approximately ~~doubling~~ doubled for the BP and tripl~~ed~~~~ng~~ for the PTFE membranes. This trend was reported in previous publications [27-29] where it was shown that increasing the flow rate has a positive impact on the total mass transfer, hence increasing the temperature polarisation coefficient. In the case of this study, since the ratio of the flux at high flow rate by the flux at low flow rate is higher for the PTFE membranes, we can conclude that the temperature polarisation had more impact on the process for the BP but that the temperature polarisation is probably not the main issue since its value is >0.9 for the range of temperatures tested. However further work is still under way to more thoroughly characterise the effects of temperature polarisation and to determine its dependency on temperature and membrane structure.[.8]

Instead of temperature polarisation, we suspect that the decline in BP membrane flux with time is due to physical ageing of the membrane including micro-crack formation, which is discussed later in greater detail. The declining flux of the BP membranes may also be linked to a progressive compaction of the membrane due to pressure from the hot and cold water streams [30-31]. A previous study has shown that the permeate pressure has an impact on the flux and membrane behaviour [3].

The flux for the BP and PTFE membranes after 2 hours of operation is plotted in Figure 8~~Figure 8~~ as a function of the hot feed temperature (top axis) and the global partial pressure difference across the membrane (bottom axis). The global partial pressure differences were calculated using the temperature in the bulk feed and permeate in the reservoirs and applying Antoine's law (Equation 3). While the reading was made as close as possible to the module, the measured temperature may still differ from the true temperature at the membrane surface due to temperature polarisation effects and potential heat losses. To distinguish this effect we refer to a "global" partial pressure difference.

The flux through the PTFE membranes is 5-12 times greater than that for the BP membranes (Figure 8~~Figure 8~~). As expected the PTFE membranes show a linear dependence on the global partial pressure difference. The slope of a linear fit to the data was calculated and multiplied by the membrane thickness to give a "global" permeability of ~21.1×10^{-12} kg/(m•s•Pa). However, in the case of the BP membranes, where a stable and steady flux is not always observed, it is difficult to accurately determine the dependence on partial pressure difference. A linear fit to the data in Figure 8~~Figure 8~~ was used to estimate a permeability on the order of

0.8×10^{-12} kg/(m•s•Pa), which is ~25 times lower than the PTFE membranes.

A number of factors may explain the lower fluxes and permeability measured for the BP membranes.

First of all, the Knudsen number for the BP and PTFE membranes were calculated to be, for the range of pore size and of temperatures between (0.48 ; 0.61), respectively, and places them in a Knüdsen/transition flow regime, with a dominant Knüdsen mode. In the Knüdsen transport regime, the permeability is directly proportional to the pore radius, making this an important parameter. Our measurements indicate that the BP membrane has pores which are an order of magnitude smaller than those of the PTFE membrane and this could therefore be an important limiting factor in BP performance. This can be addressed in the future by tailoring the pore size distribution of the BP membranes. Work previously done by us showed that mixing CNTs of different diameter would lead to different structures and average pore size [32] and it was also shown that porosity could be tailored by using polymeric templates inside the structure of BPs [33].

A second possible reason for the difference in flux rate and permeability may be the distinctly different structure of the two membranes. While the PTFE membrane has more conventional pores, which traverse the entire membrane thickness, the BP pores are defined by an interconnected network of CNTs (Figure 4~~Figure 4~~). The BP structure is therefore closer to that of a non-woven fabric and the concept of a cylindrical pore not an appropriate simplification. This interconnected CNT network also results in a very high surface area, ~20 times greater than that for PTFE. This could lead to an increased number of molecular-wall collisions and hence a more tortuous path for water vapour through the BP membrane reducing permeability. A tortuosity factor of 2 was assumed for both membranes in the theoretical calculations [15].

The most important outcome of this work is that self-supporting BP membranes were successfully operated in a DCMD setup to desalinate synthetic seawater. A flux on the order of 5 - 25 kg/m^2•h was measured for “global” vapour pressure differences between 10-40 kPa. This is encouraging given that the BP membranes were in no way supported and that no binding agents were used in their construction. The CNTs within the BP membrane are held together solely by Van der Waals interactions.

4.2.2 Membrane integrity for salt rejection

Membrane integrity is an important parameter affecting both membrane lifetime and performance. The integrity of the BP membranes was investigated in two ways. Firstly, the conductivity of the cold reservoir was monitored with time. If only water vapour crosses the membrane, then the electrical conductivity of the cold solution should progressively decrease in proportion to the amount of water transferred. PTFE membranes show this exact behaviour,

representing close to 100% salt rejection (Figure 11~~Figure 11~~). In contrast, most BP membranes showed a very slight but progressive increase in conductivity corresponding to desalination efficiencies between 88 and 99% as shown in Table 2. Furthermore, after 4 to 7 hours of testing a rapid increase in conductivity was typically observed for the BP membranes indicating that liquid water was breaching the membrane allowing salt passage from the hot to the cold stream

Secondly, the membranes were characterised after testing in the MD setup by milling sections through the BP with a Focused Ion Beam milling followed by SEM imaging. As shown in Figure 12~~Figure 12~~, micro-cracks were present and seem to represent regions of delamination between the CNT layers. These micro-cracks likely develop during MD testing and eventually form a direct bridge from the feed to permeate, leading to the rapid increase in permeate conductivity mentioned above. This is further supported through EDX analysis which confirmed the presence of sodium and chloride within the micro-cracks, while none was detected in regions away from the cracks. It is suspected that the ageing of these membranes is accelerated due to the MD setup which incorporated two pulsating peristaltic pumps. This causes an oscillation of the membranes, and potentially delamination of sheets nanotubes as they are held together solely through Van der Waals forces [34-35]. It is likely that the gradual formation of micro-cracks contributes to the loss of flux observed during operation for the BP membranes. Various approaches, such as composite structures and the addition of polymers are currently being investigated to avoid the formation of cracks.

5. CONCLUSIONS

CNT BP membranes were fabricated by vacuum filtration and characterised to determine their suitability for MD. They were found to have many properties favourable for MD. For example they exhibit a high contact angle (113 degrees), high porosity (90%), and relatively low thermal conductivity of 2.7 kW/m^2•h. These properties are better than most of polymeric membranes conventionally used in MD and compare well with PTFE membranes.

Most importantly desalination was successfully demonstrated using CNT BP membranes in a DCMD setup. The best results gave 99% salt rejection and a flux rate of 12 kg/m^2•h at a water vapour partial pressure difference of 22.7 kPa. Some issues were encountered during DCMD testing such as a decline in flux with time and delamination of BP membranes due to the formation of micro cracks. Lifespan of the BP membranes is still inferior to PTFE membranes. However it is important to stress that these BP membranes were not supported and were composed solely by CNTs. Work is currently underway to optimise the BP membranes with an emphasis on supported and composite structures for improved lifetime and permeability. The pore size of BP membrane can be tailored and work is currently done to have engineered pore size distribution while keeping high porosity membranes.

In summary, carbon nanotube based membranes have many physical and surface properties beneficial for MD. This work was a proof of concept that CNT structures are suitable for water desalination. Our results to date indicate that BP membranes are a promising alternative to current polymeric membranes although further work is needed to fully understand and optimise their properties for MD.

ACKNOWLEDGMENTS

The author would like to thank the Commonwealth Scientific Industrial and Research Organization (CSIRO) Materials Science and Engineering and the Institute for Sustainability and Innovation at Victoria University for financial support. We also wish to acknowledge the expert advice and assistance of Dr. John Ward and Mark Greaves on SEM, and Dr. Sergey Rubanov and Dr. Kenneth Goldie for focused ion beam milling. We would also like to thank Zongli Xie and Lisa Wong for their help with BET measurements, Dr. Julie Nigro for her advice with the fluorescence tests, Dr. Shane Cox, from UNSW – Australia, for his assistance with Porometer measurements and finally, Dr. Jun De-Li and Jianhua Zhang, from Victoria University - Australia, for their assistance with heat conductivity tests.

LIST OF FIGURES

LIST OF TABLES:

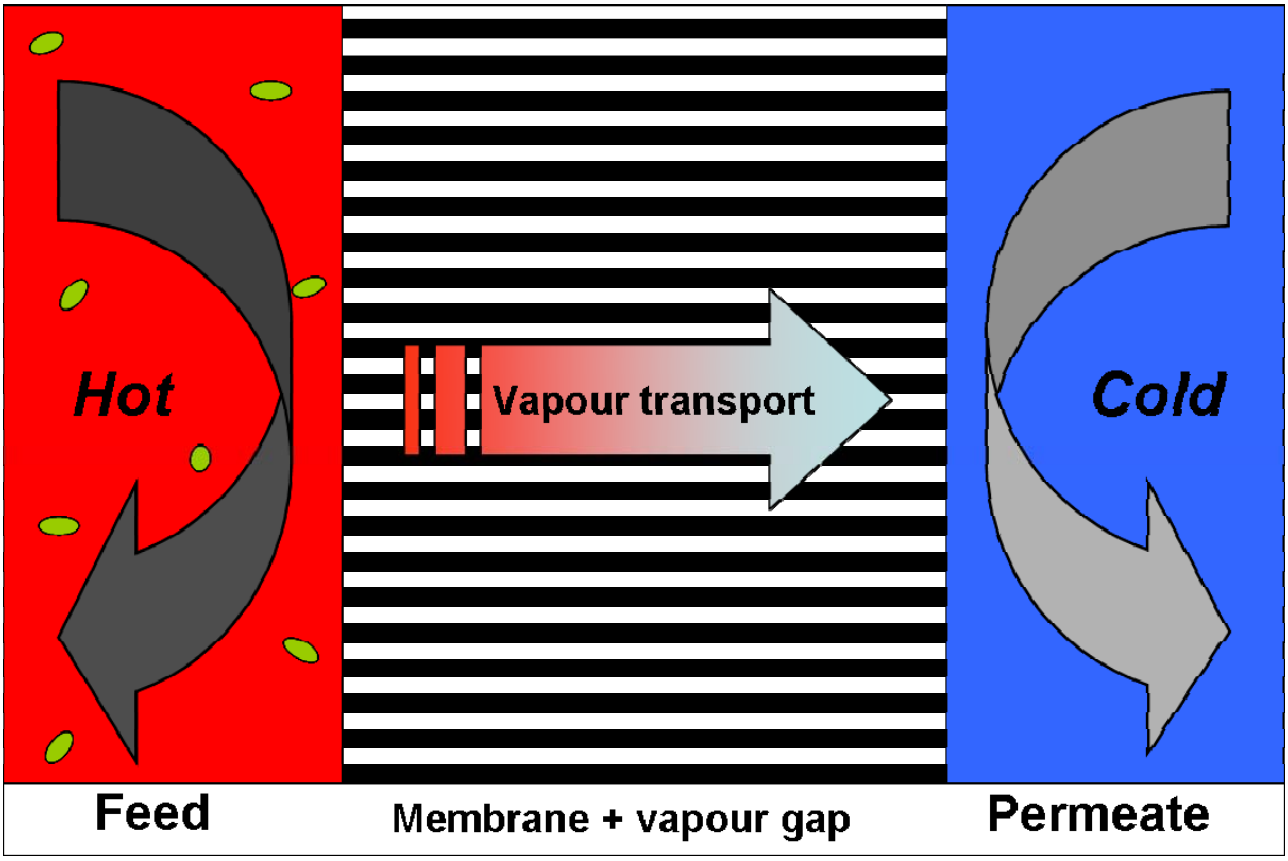

Figure 1 Schematic showing the concept behind Direct Contact Membrane Distillation.

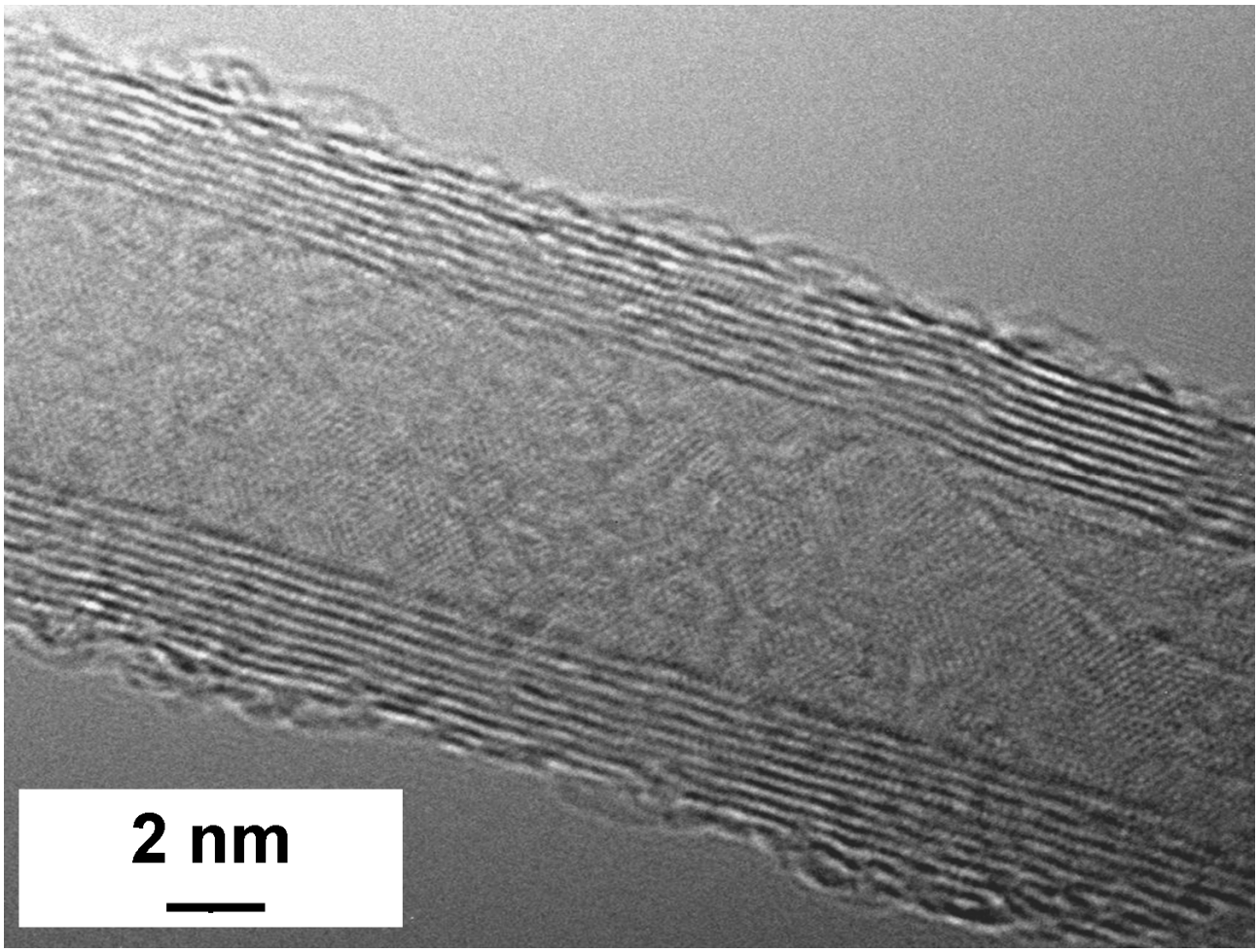

Figure 2 TEM image of a multiwalled CNT showing a number of concentric walls.

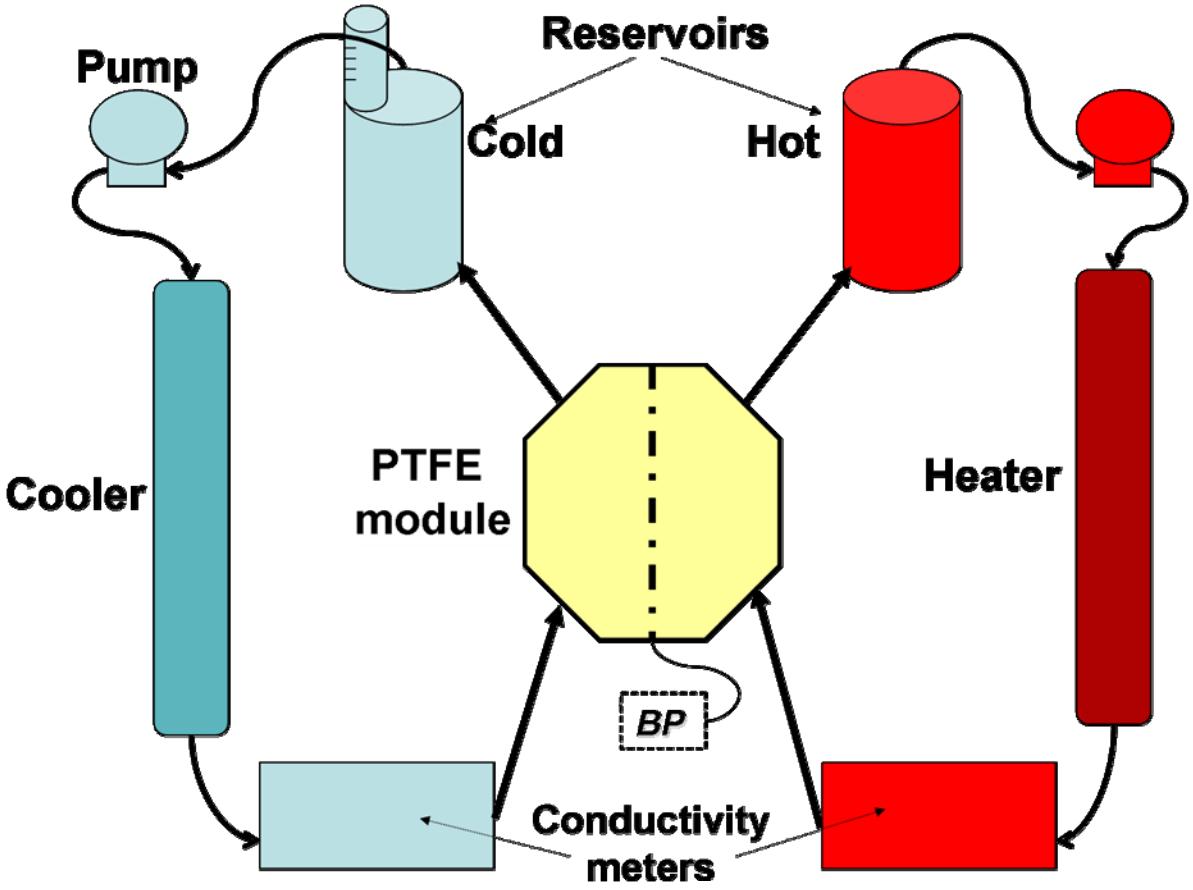

Figure 3 of the Direct Contact Membrane Distillation test rig.

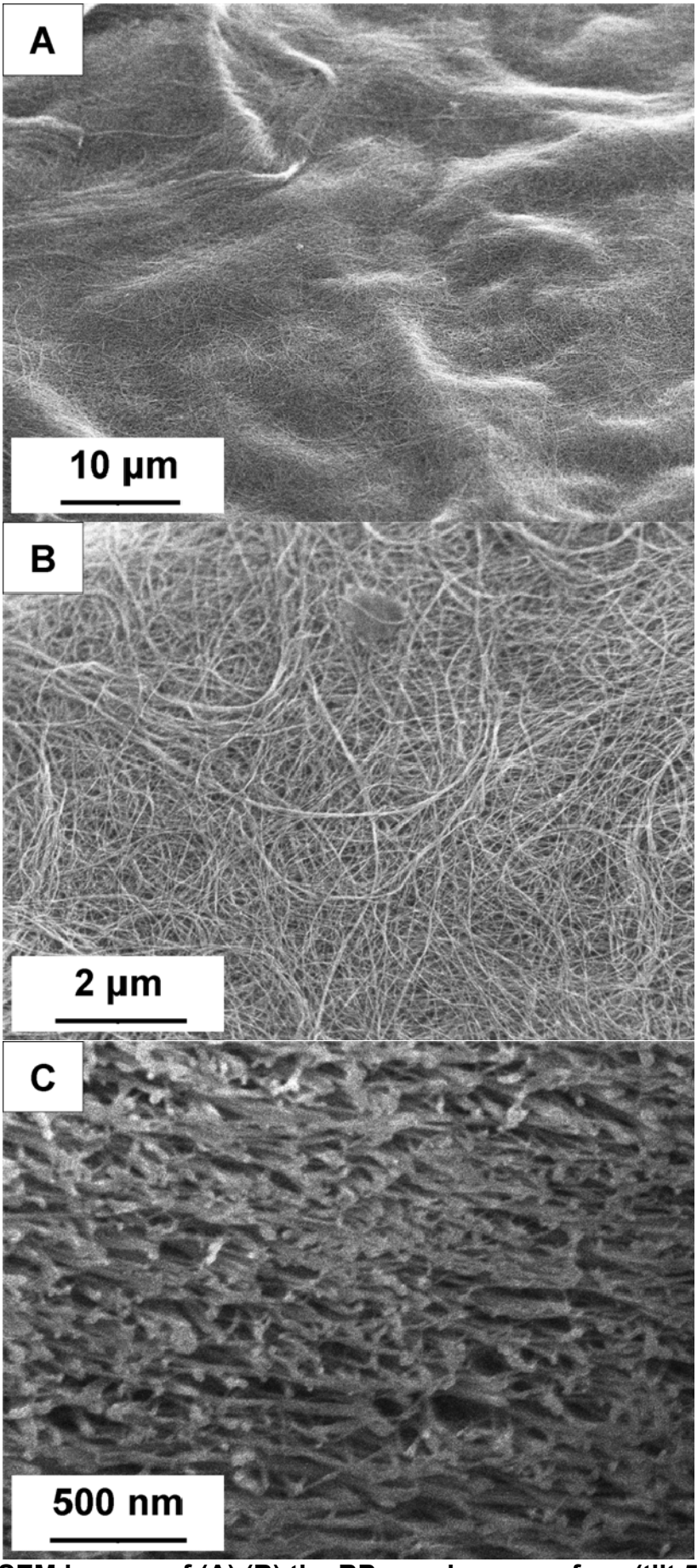

Figure 4 SEM images of (A),(B) the BP membrane surface (tilt 52º and 0º respectively), (C) a cross section milled using the focused ion beam (tilt 52º).

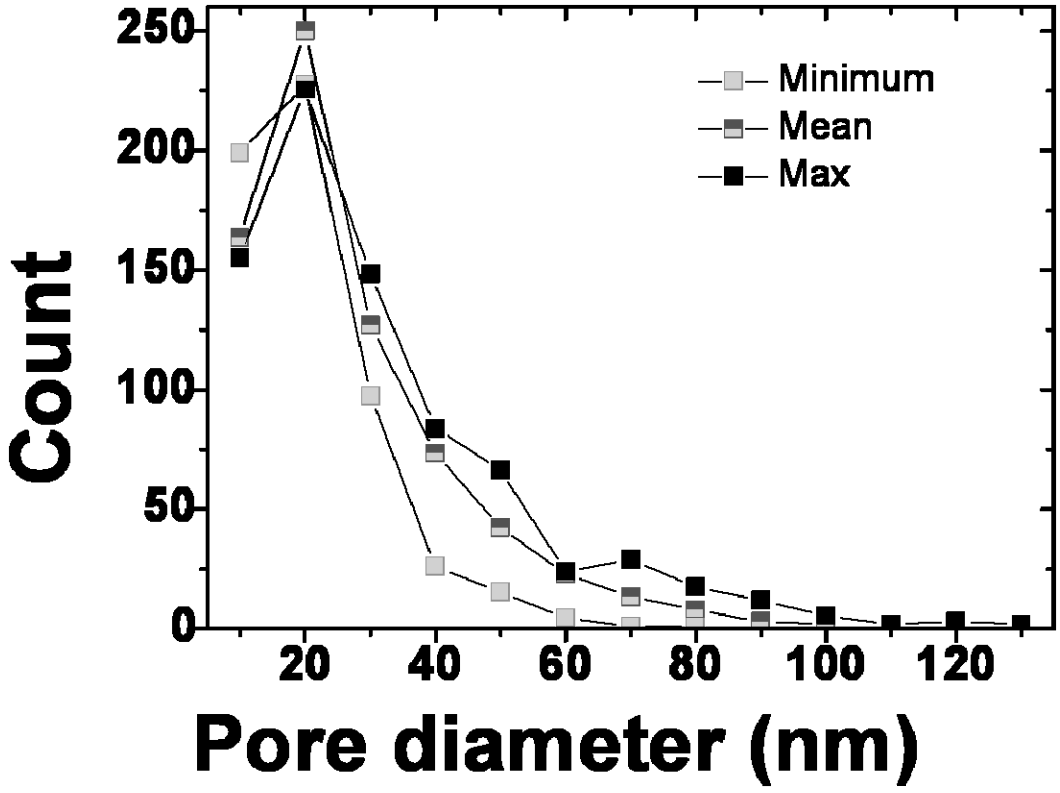

Figure 5 Pore size distribution of the BP membrane as determined by SEM imaging of the surface. Minimum, mean and maximum Feret pore diameters were defined as the average values over the surface of the studied SEM images. Each pore was defined by a combination of 3 vectors

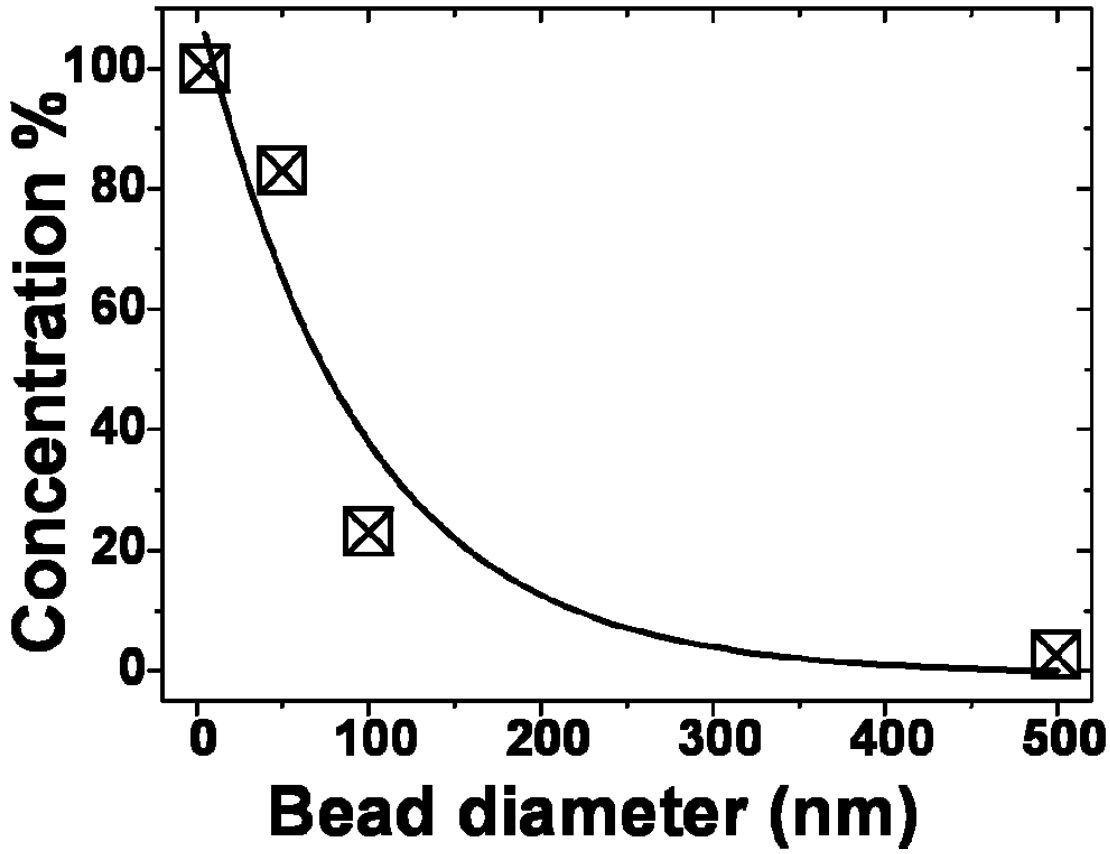

Figure 6 Pore size selectivity determined from particle exclusion tests.

[dum025 9]

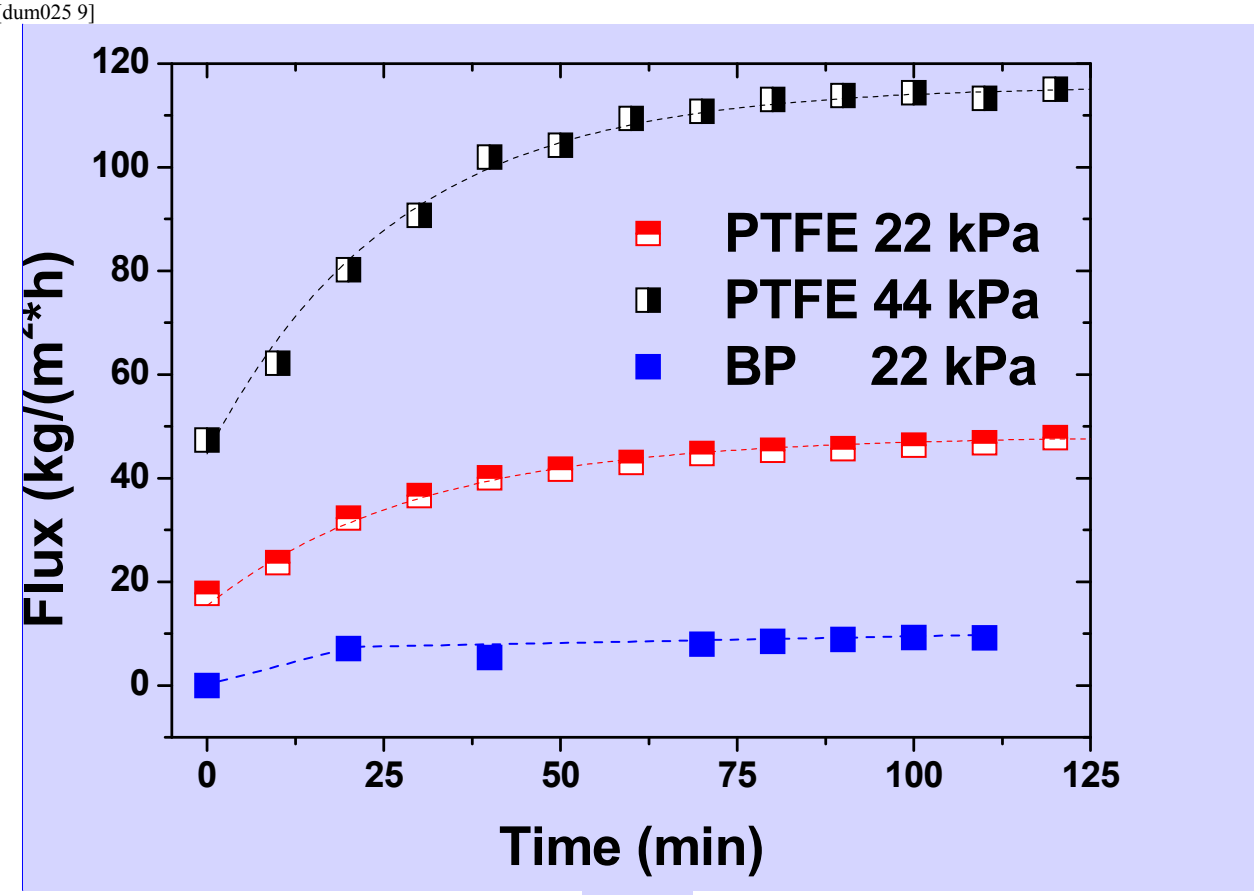

[dum025 10]

Figure 7 Representative curves for BP and PTFE membranes showing the variation in flux with time. The data was acquired for a cold and hot side flow rate of 300 ml/h, and an initial hot-side conductivity of ~ 10 μS•cm^{-1}. The working temperatures used in the experiments corresponded to various global vapour pressure differences: at 22 kPa (Hot: 65ºC; Cold: 5ºC); at 44 kPa (Hot: 77ºC; Cold: 5ºC)

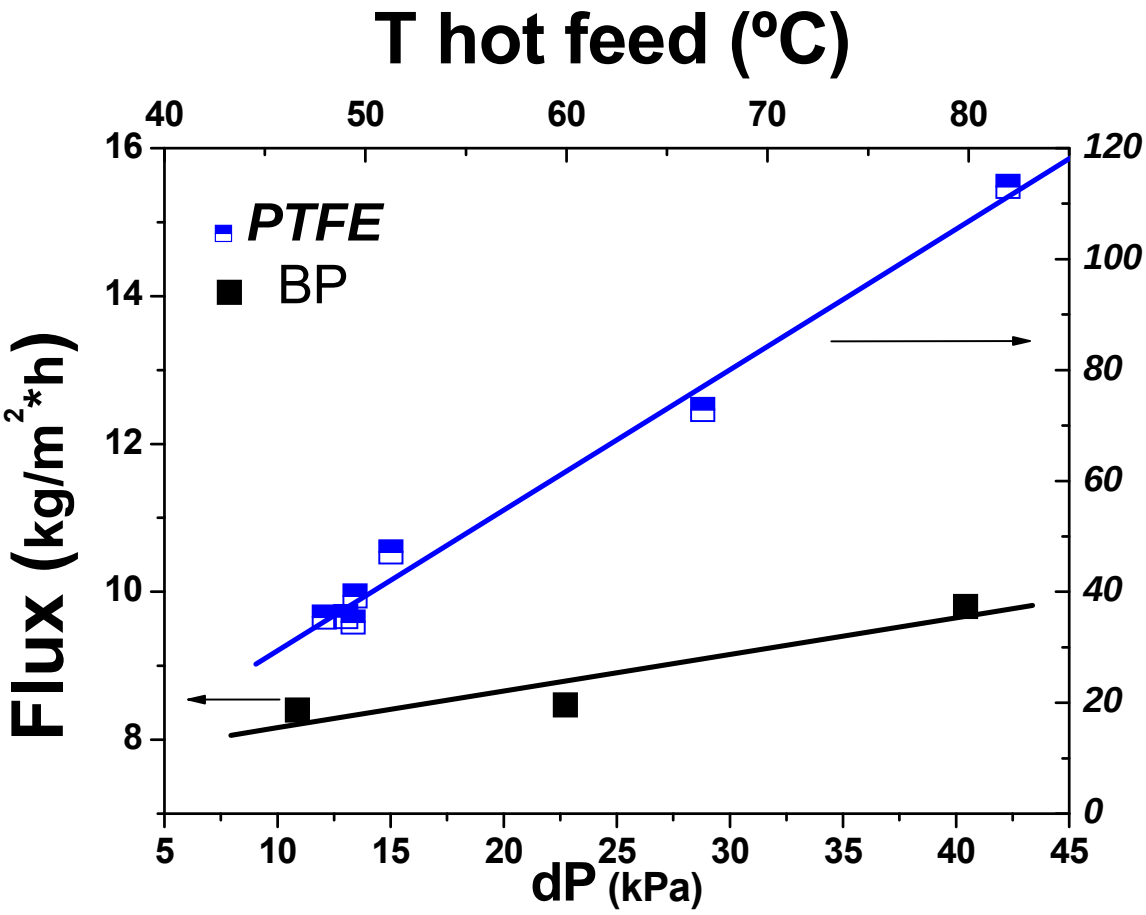

Figure 8 Dependence of flux on global vapour pressure difference, ΔP, for the BP (black curve, left Y axis) and PTFE (grey curve, right Y axis) membranes.

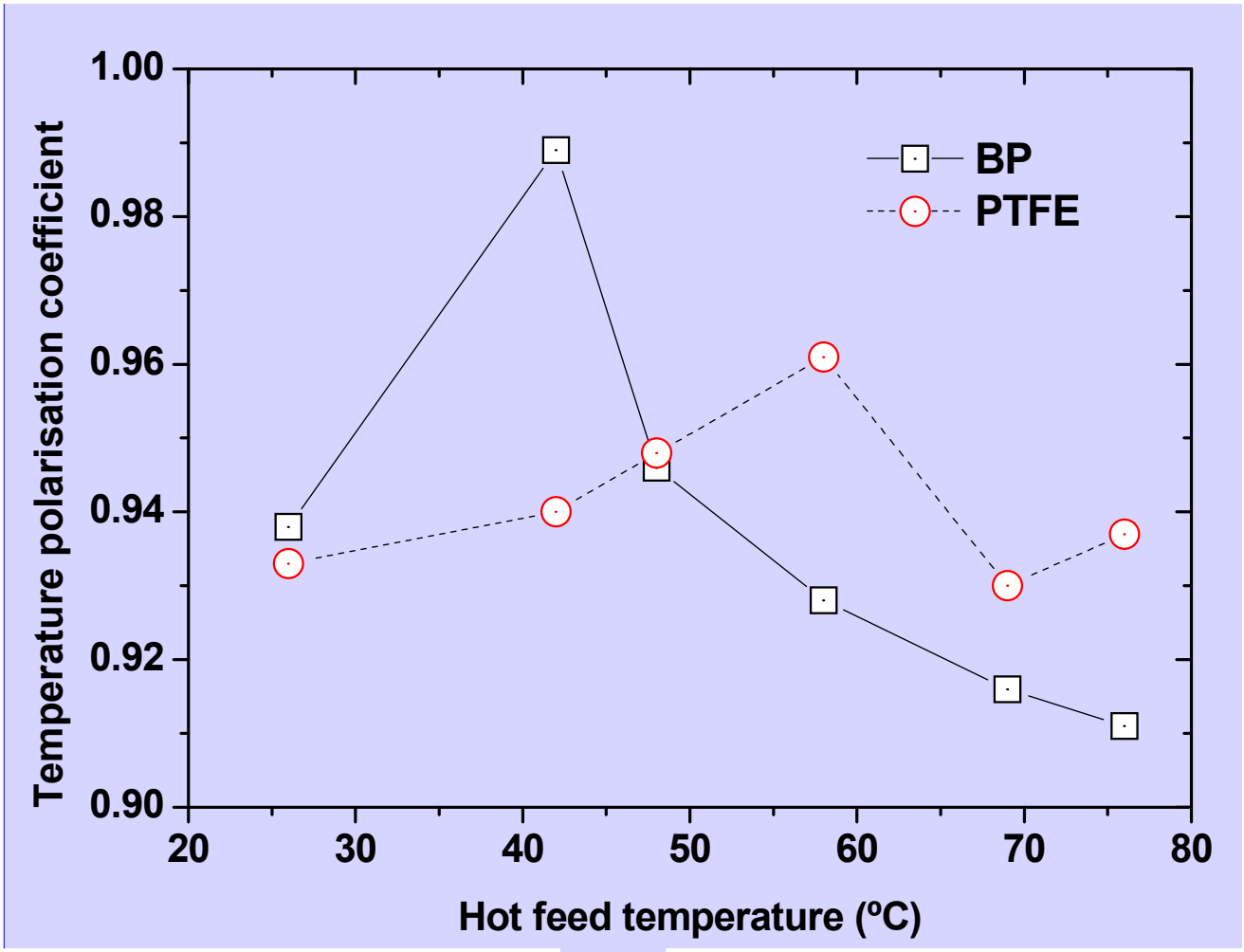

[dum025 11]

Figure 9 Temperature polarisation as a function of feed temperature. The test conditions were kept similar as a classical DCMD test.

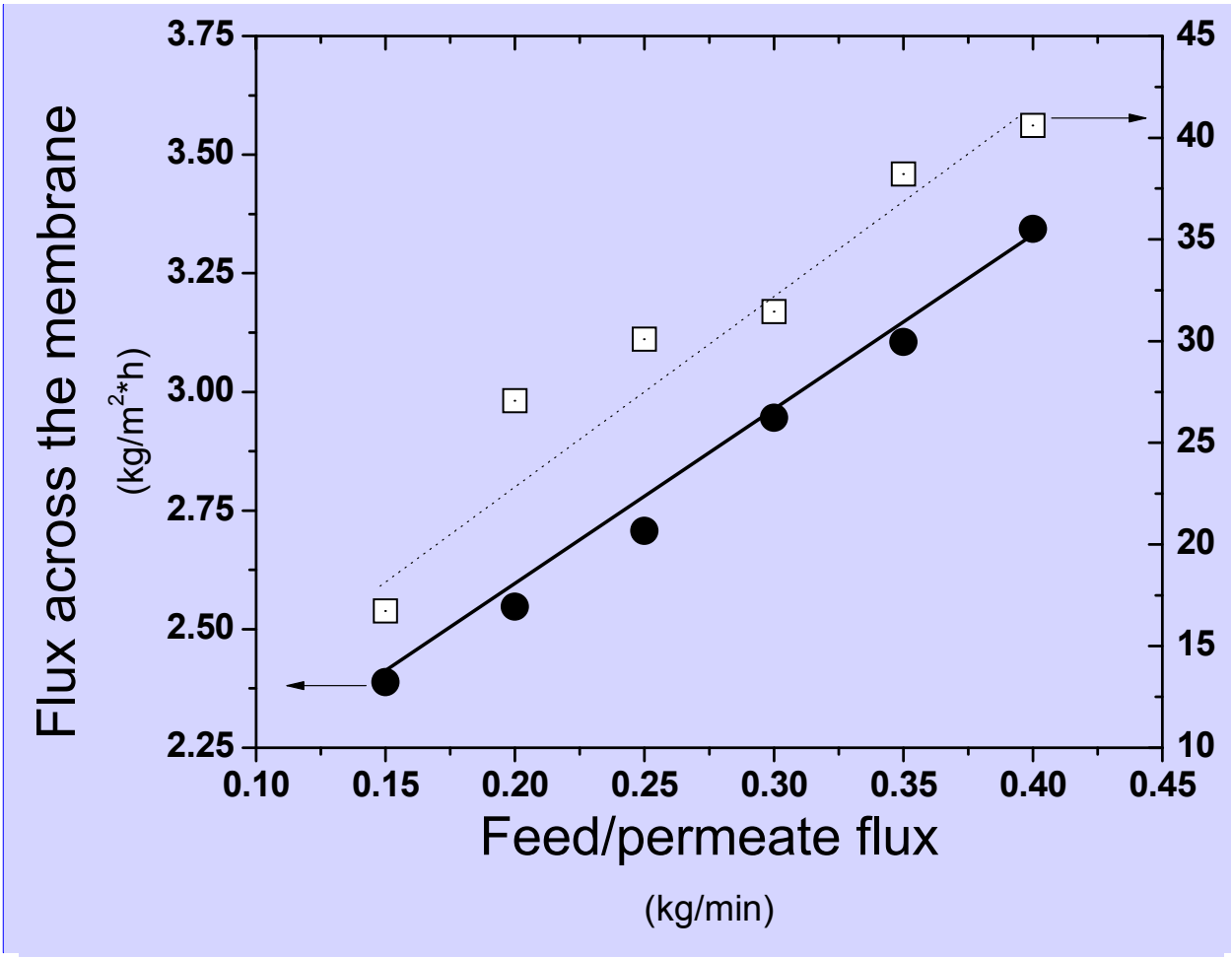

Figure 10 Flux of pure water across the membranes for changing feed/permeate flow rates. Plain circles (left Y axis) and empty squares (right Y axis) respectively stand for bucky-paper and PTFE membranes. The average ~~desalination~~ rejection rate was ~90% for the BP while the thickness of the tested sample was ~110μm. The tests were performed ~~on~~ for at least 1h and with a hot temperature of 80ºC and a cold temperature of 5ºC. ~~Both lines are given for the guideline of the eye.~~

[dum025 12]

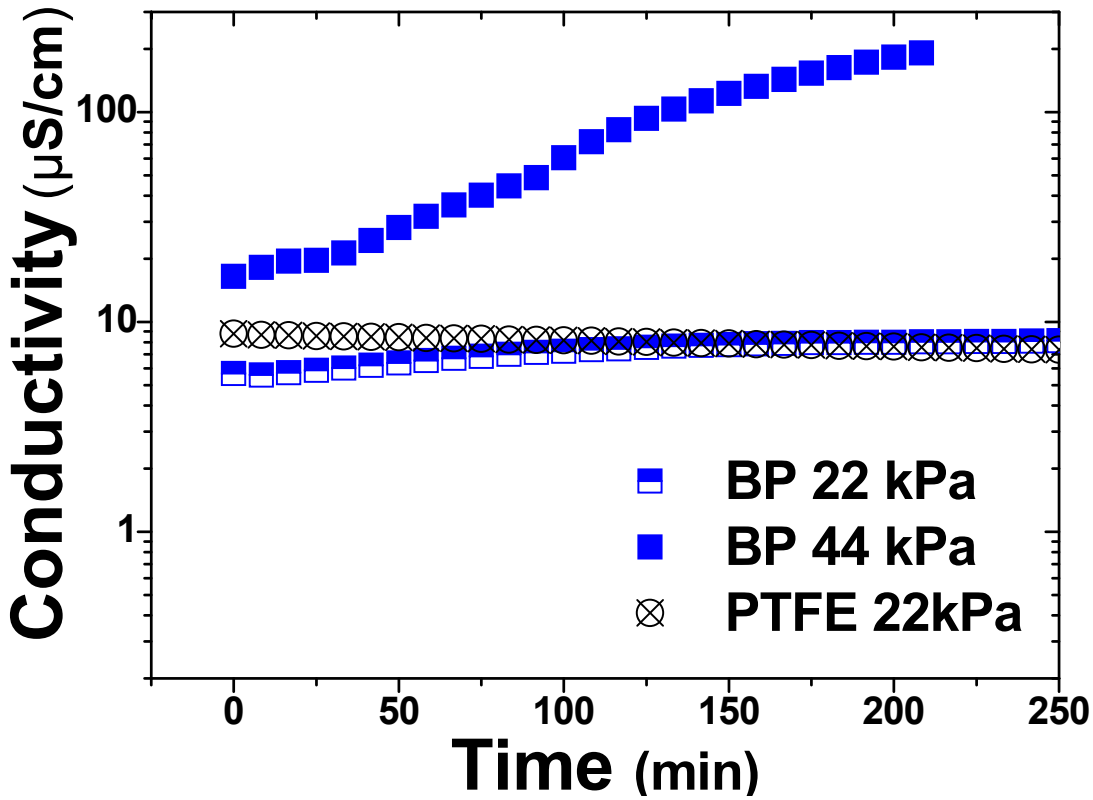

Figure 11 Representative conductivity curves recorded for the cold permeate side as a function of time. The conductivity of the hot stream was ~ 11 mS.

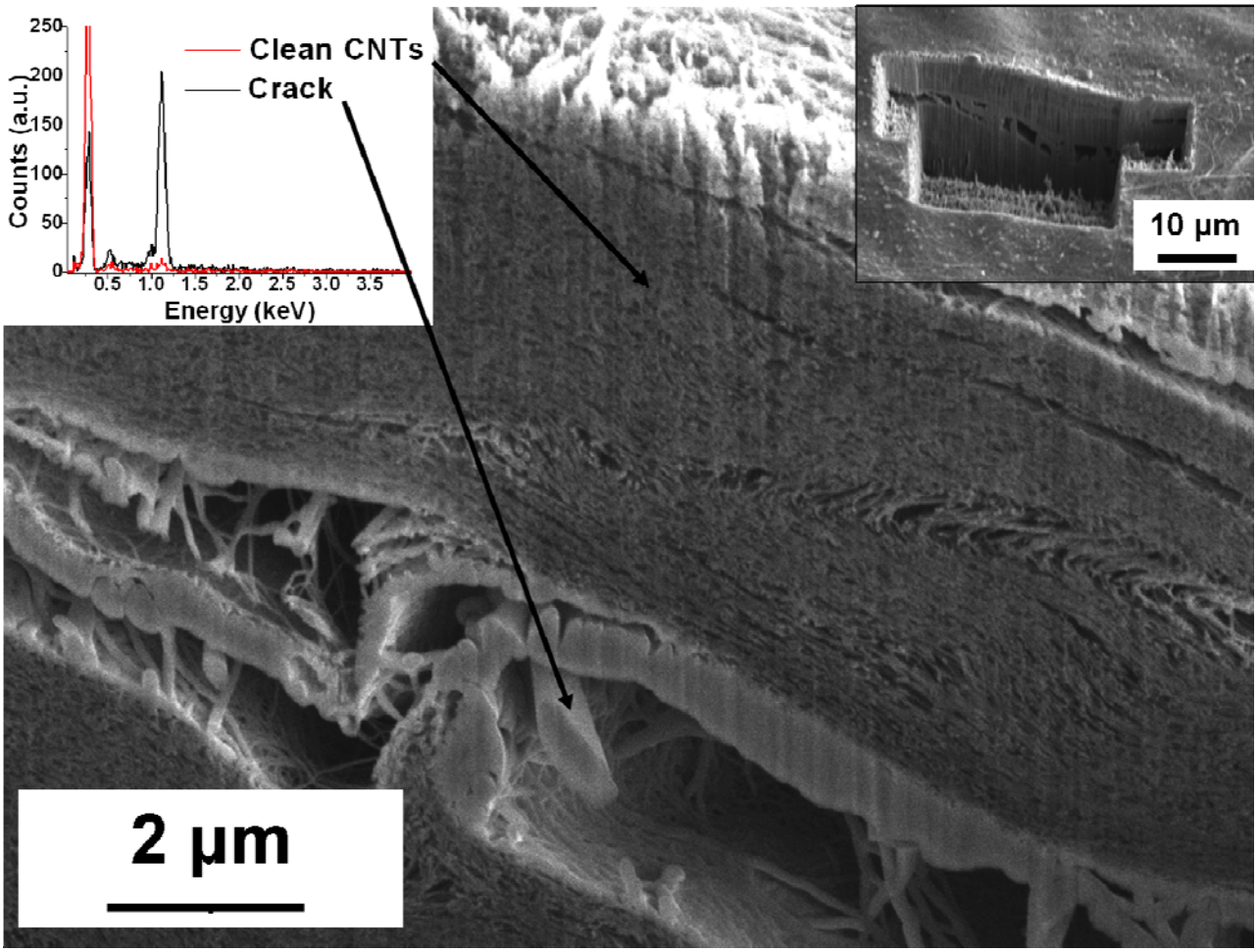

Figure 12 SEM images at 5 keV and 7.5 mm w.d. showing a cross-section through a BP membrane after testing. The section was milled with a focused ion beam and the image was taken at a 52° tilt. The left inset shows EDX curves taken inside and well away from the crack. The right inset shows a low magnification view of the cross section

Table 1 Summary of characterisation results for the BP and PTFE membranes

Property	Units	BP	PTFE
Pore Size (nm)			
*SEM Minimum**	nm	20.69 (10.27)	-
*SEM Mean**		27.28 (16.7)	220[++]
*SEM Maximum**		32.37 (22.5)	-
Porometer Mean		44	548
*Cut-off***		50-100	500[+]
Porosity	%	90	70
BET surface area	m^2/g	197	21
Thermal conductivity	$W/(m^2*K)$	2.3	0.25
Density	kg/m^3	232.5	293.8
Mechanical tensile specific modulus[+]	$GPa*m^3/g$	5.27	-
Contact angle	º	113.3	120.4
Bubble point	kPa	37.92	99.9[++]
Liquid entry pressure	kPa	55.15	344.7

*Value given in brackets is the standard deviation
** For 90% rejected particles
[+] Thickness of test was 5 µm (±0.2 µm)
[++]Data taken from Millipore specification data sheet

Table 2 Membrane properties, test conditions and rejection efficiency

Membrane	Mass (mg)	Thickness (μm)	T_{ave} (°C)	ΔT (°C)	ΔP (kPa)	Rejection (%)
PTFE	20.9 (8.61)	205 (30)*	41	29.1	12.7	100
			32	46.8	15.02	100
			39	59.5	28.81	100
			45	65.9	42.29	100
BP	4.75	45	27	41.2	10.89	99.99
	6.65	55	45	63.8	40.43	88.46
	7.98	42	36	53.2	22.73	94.08

* the thickness of the complete structure is ~205 μm while the active layer is ~30 μm thick.

References

[1] El-Bourawi, M.S., Z. Ding, R. Ma, and M. Khayet, *A framework for better understanding membrane distillation separation process.* Journal of Membrane Science, 2006. **285**(1-2): p. 4-29.

[2] Lawson, K.W. and D.R. Lloyd, *Membrane distillation. II. Direct contact MD.* Journal of Membrane Science, 1996. **120**(1): p. 123-133.

[3] Lawson, K.W. and D.R. Lloyd, *Membrane distillation.* Journal of Membrane Science, 1997. **124**(1): p. 1-25.

[4] Khayet, M. and T. Matsuura, *Preparation and Characterization of Polyvinylidene Fluoride Membranes for Membrane Distillation.* Industrial & Engineering Chemistry Research, 2001. **40**(24): p. 5710-5718.

[5] Smolders, K. and A.C.M. Franken, *Terminology for Membrane Distillation.* Desalination, 1989. **72**(3): p. 249-262.

[6] Gryta, M., M. Tomaszewska, and K. Karakulski, *Wastewater treatment by membrane distillation.* Desalination, 2006. **198**(1-3): p. 67-73.

[7] Basmadjian, D., *Mass transfer: principles and applications*. 2004.

[8] Corry, B., *Designing Carbon Nanotube Membranes for Efficient Water Desalination.* The Journal of Physical Chemistry B, 2008. **112**(5): p. 1427-1434.

[9] Fornasiero, F., H.G. Park, J.K. Holt, M. Stadermann, C.P. Grigoropoulos, A. Noy, and O. Bakajin, *Ion exclusion by sub-2-nm carbon nanotube pores.* Proceedings of the National Academy of Sciences of the United States of America, 2008. **105**(45): p. 17250-17255.

[10] Hinds, B.J., N. Chopra, T. Rantell, R. Andrews, V. Gavalas, and L.G. Bachas, *Aligned multiwalled carbon nanotube membranes.* Science, 2004. **303**(5654): p. 62-65.

[11] Holt, J.K., H.G. Park, Y.M. Wang, M. Stadermann, A.B. Artyukhin, C.P. Grigoropoulos, A. Noy, and O. Bakajin, *Fast mass transport through sub-2-nanometer carbon nanotubes.* Science, 2006. **312**(5776): p. 1034-1037.

[12] Muramatsu, H., T. Hayashi, Y.A. Kim, D. Shimamoto, Y.J. Kim, K. Tantrakarn, M. Endo, M. Terrones, and M.S. Dresselhaus, *Pore structure and oxidation stability of double-walled carbon nanotube-derived bucky paper.* Chemical Physics Letters, 2005. **414**(4-6): p. 444-448.

[13] Bessieres, A., M. Meireles, R. Coratger, J. Beauvillain, and V. Sanchez, *Investigations of surface properties of polymeric membranes by near field microscopy.* Journal of Membrane Science, 1996. **109**(2): p. 13.

[14] Burgoyne, A. and M.M. Vahdati, *Direct Contact Membrane Distillation.* Separation Science and Technology, 2000. **35**(8): p. 1257 - 1284.

[15] Phattaranawik, J., R. Jiraratananon, and A.G. Fane, *Effect of pore size distribution and air flux on mass transport in direct contact membrane distillation.* Journal of Membrane Science, 2003. **215**(1-2): p. 75-85.

[16] Schofield, R.W., A.G. Fane, C.J.D. Fell, and R. Macoun, *Factors Affecting Flux in Membrane Distillation.* Desalination, 1990. **77**(1-3): p. 279-294.

[17] Bird, R.B., W.E. Stewart, and E.N. Lightfoot, *Transport Phenomena, Revised 2nd Edition*. 2006, New Yor/Chichester/Weinheim/Brisbane/Singapore/Toronto: John Wiley & Sons, Inc.

[18] Huynh, C. and S. Hawkins, *Understanding the synthesis of directly spinnable carbon nanotube forests.* Submitted to Carbon, 2009.

[19] Gou, J., Z.Y. Liang, and B. Wang, *Experimental Design and Optimization of Dispersion Process for Single-Walled Carbon Nanotube Bucky Paper.* International Journal of Nanoscience, 2004. **3**(3): p. 14.

[20] Hernández, A., J.I. Calvo, P. Prádanos, and F. Tejerina, *Pore size distributions in microporous membranes. A critical analysis of the bubble point extended method.*

Journal of Membrane Science, 1996. **112**(1): p. 1-12.
[21] Cooper, S.M., H.F. Chuang, M. Cinke, B.A. Cruden, and M. Meyyappan, *Gas Permeability of a Buckypaper Membrane.* Nano Letters, 2003. **3**(2): p. 189-192.
[22] Nuriel, S., L. Liu, A.H. Barber, and H.D. Wagner, *Direct measurement of multiwall nanotube surface tension.* Chemical Physics Letters, 2005. **404**(4-6): p. 263-266.
[23] Smajda, R., A. Kukovecz, Z. Konya, and I. Kiricsi, *Structure and gas permeability of multi-wall carbon nanotube buckypapers.* Carbon, 2007. **45**(6): p. 1176-1184.
[24] Shinde, S.L. and J. Goela, *Unusually high thermal conductivity of carbon nanotubes*, in *High Thermal Conductivity Materials*, Springer, Editor. 2004. p. 40.
[25] Gonnet, P., Z. Liang, E.S. Choi, R.S. Kadambala, C. Zhang, J.S. Brooks, B. Wang, and L. Kramer, *Thermal conductivity of magnetically aligned carbon nanotube buckypapers and nanocomposites.* Current Applied Physics, 2006. **6**(1): p. 119-122.
[26] Cabassud, C. and D. Wirth. *Membrane distillation for water desalination: how to chose an appropriate membrane?* in *Conference on Desalination and the Environment - Fresh Water for All*. 2003. Malta, Italy: Elsevier Science Bv.
[27] Rivier, C.A., M.C. García-Payo, I.W. Marison, and U. von Stockar, *Separation of binary mixtures by thermostatic sweeping gas membrane distillation: I. Theory and simulations.* Journal of Membrane Science, 2002. **201**(1-2): p. 1-16.
[28] Matheswaran, M., T.O. Kwon, J.W. Kim, and I.S. Moon, *Factors affecting flux and water separation performance in air gap membrane distillation.* Journal of Industrial Engineering chemistry, 2007. **13**(6): p. 5.
[29] Zhang, J., N. Dow, M. Duke, E. Ostarcevic, J.-d. Li, and S. Gray, *Identification of material and physical features of membrane distillation membranes for high performance desalination.* Journal of membrane science, 2010.
[30] Laganà, F., G. Barbieri, and E. Drioli, *Direct contact membrane distillation: modelling and concentration experiments.* Journal of Membrane Science, 2000. **166**(1): p. 1-11.
[31] Lawson, K.W., M.S. Hall, and D.R. Lloyd, *Compaction of microporous membranes used in membrane distillation. I. Effect on gas permeability.* Journal of Membrane Science, 1995. **101**(1-2): p. 99-108.
[32] Dumée, L., K. Sears, J. Schütz, N. Finn, M. Duke, and S. Gray. *Design and Characterisation of Carbon Nanotube Bucky-Paper Membranes for Membrane Distillation*
in *ICOM08*. 2008. Honolulu - Hawaii, USA.
[33] Das, R.K., B. Liu, J.R. Reynolds, and A.G. Rinzler, *Engineered Macroporosity in Single-Wall Carbon Nanotube Films.* Nano Letters, 2009. **9**(2): p. 677-683.
[34] Chandler, D., *Interfaces and the driving force of hydrophobic assembly.* Nature, 2005. **437**(7059): p. 640-647.
[35] Parsegian, V.A., *Van der Waals Forces: A Handbook for Biologists, Chemists, Engineers, and Physicists*. 2005: Cambridge University Press.

…
…
…
LAST PAGE